

## Vacuum fluorescent displays utilizing ZnO nanoparticles

Charles H. Aaronson,<sup>1,a)</sup> Hiro Amekura (雨倉宏),<sup>1,b)</sup> Yoshitaka Sato (佐藤義孝),<sup>2</sup> and Naoki Kishimoto (岸本直樹)<sup>1</sup>

<sup>1</sup>National Institute for Materials Science, 3-13 Sakura, Tsukuba, Ibaraki 305-0003, Japan

<sup>2</sup>Futaba Corporation, 1080 Yabutsuka, Chosei-mura, Chosei-gun, Chiba 299-4395, Japan

(Received 14 September 2010; accepted 3 December 2010; published online 20 January 2011)

Zinc-oxide (ZnO) nanoparticles (NPs) fabricated by ion implantation combined with thermal oxidation were installed into vacuum fluorescent displays. The cathode-ray induced luminescence observed was strongly dependent on sample oxidation temperature. Raising the temperature from 650 to 800 °C, the relative intensity of the defect band around 480 nm to that of the free-exciton recombination at 380 nm increased. With increasing accelerating voltage, the free-exciton peak of ZnO NPs shifted to a longer wavelength. This was ascribed to a temperature increase due to cathode ray irradiation because the shift was only observed during continuous wave mode operation and not during pulsed mode operation. As the oxidation temperature was further raised to 900 °C strong green band emission around 520 nm became the only luminescence band. This was due to the formation of the Zn<sub>2</sub>SiO<sub>4</sub> phase from the reaction between ZnO NPs and the SiO<sub>2</sub> substrate, which was confirmed by x-ray diffraction, x-ray photoelectron spectroscopy, and optical absorption spectroscopy. © 2011 American Institute of Physics. [doi:10.1063/1.3536631]

### I. INTRODUCTION

Over the past decade the fabrication of nanoparticle (NP) based optoelectronic devices has advanced considerably. The ability to use such technologies to augment and replace conventional electronic components is becoming far more viable both in terms of cost and manufacturing techniques.

One of the most promising new developments in this field is vacuum fluorescent displays (VFDs) (Ref. 1) which are based on the use of zinc-oxide (ZnO) NPs as the light emitting component rather than conventional phosphors such as ZnO:Zn micropowder.<sup>2,3</sup> These NP displays have a number of significant advantages. One of the substantial benefits is a direct consequence of the nanometer-sized light emitting particles. At this size ZnO NPs are smaller than the wavelength of visible light and thus fully transparent. This is a considerable innovation as traditional phosphor displays consist of micrometer-size powder and are therefore *opaque*. This limits their use in certain applications. Further, these devices have the ability to operate efficiently at much higher temperatures than p-n junction based light emitting diodes. These two advantages allow for such devices to be used in applications where traditional components cannot be employed. For example, consider the notion of using a ZnO NP VFD as an automobile turn signal implanted within a car window or as warning bulb in devices that are required to function outside the operating temperature range of conventional LEDs.

Over the past years Amekura *et al.*<sup>4</sup> have advocated ion implantation combined with thermal oxidation as a successful route for the fabrication of oxide NPs. Further, they have demonstrated that this technique leads to the formation of

ZnO NPs which are highly compatible and homogeneous within a given substrate. In this paper, ZnO NPs were mounted into the VFD structure and the performance of these NP VFDs was tested in terms of light-emitting properties.

The manufacturing processes of such NP devices, although currently high cost on a small scale, have the potential to be mass marketed to produce NP VFDs on a competitive cost basis. With the advantages discussed above, it is an exciting prospect to consider the future of such NP based VFDs in consumer electronics.

### II. EXPERIMENTAL

Optical-grade silica glass (SiO<sub>2</sub>) disks of the KU-1 type (OH<sup>-</sup> ~ 820 ppm), 0.5 mm in thickness, were implanted with <sup>64</sup>Zn<sup>+</sup> ions at 60 keV to a fluence of 1.0 × 10<sup>17</sup> ions/cm<sup>2</sup>. The samples showed brownish color after implantation indicating the formation of metallic Zn NPs.<sup>5,6</sup> The Zn NPs were then oxidized in oxygen gas at a pressure of ~1 atm in a tube furnace at temperatures of 650, 750, 800, and 900 °C. The duration for the thermal oxidation was 1 h for 650, 750, and 800 °C and 1.5 h for 900 °C. After annealing, all the samples showed full transparency, consistent with the transformation to ZnO NPs or the secondary Zn<sub>2</sub>SiO<sub>4</sub> phase.<sup>7</sup> Cross-sectional TEM confirmed that the implanted side of the silica substrate was fully covered by discrete ZnO NPs of semispherical shape (at 650, 750, and 800 °C), or by a continuous layer of Zn<sub>2</sub>SiO<sub>4</sub> (at 900 °C).<sup>6</sup> These disks were then encased in sample VFD containers and connected according to Fig. 1(a).

The VFD structure consisted of each oxidized sample contained within a fabricated glass case as shown in Fig. 1(b). This case was then connected to four power sources in accordance with the schematic in Fig. 1(a). First was a current, used to heat up three sets of filaments inducing thermal

<sup>a)</sup>On leave from Imperial College London, Department of Materials as part of IAESTE technical exchange program.

<sup>b)</sup>Electronic mail: amekura.hiroshi@nims.go.jp.

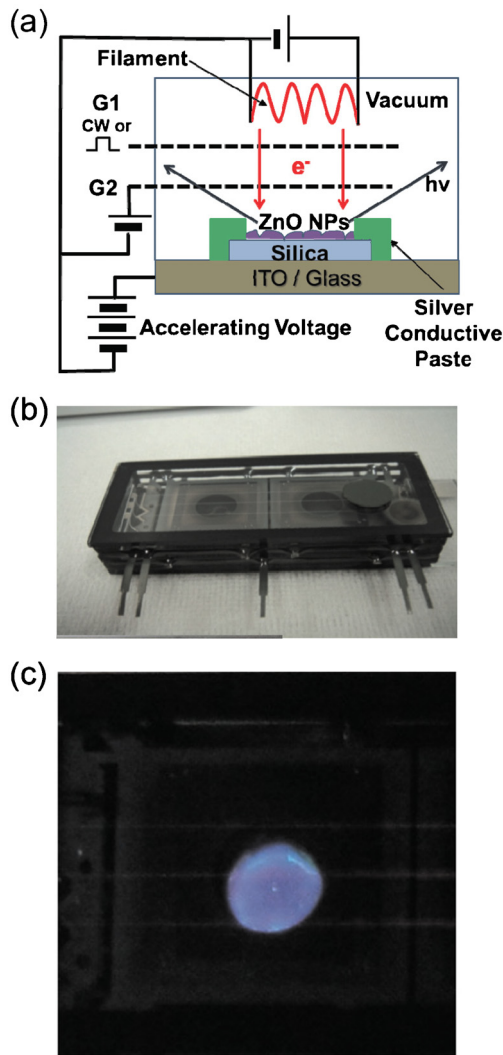


FIG. 1. (Color online) (a) Schematic cross section through the enclosed luminescence device showing all sample connections. (b) Sample within prepared substrate displaying connection terminals. (c) Blue luminescence observed at an accelerating voltage of 1500 V for sample oxidized at 650 °C

electron emission. Edges of the sample were connected to the anode by means of silver conductive paste in order to apply an accelerating voltage up to 3000 V. In addition, two gate voltages (G1 and G2) were used to control the flow of electrons toward the sample. With voltages applied across the gates, electrons were able to flow and interact with the ZnO NPs leading to the luminescence shown in Fig. 1(c). Since VFDs are based on vacuum tubes, relatively low voltages of 5–10 V on G1 and G2 could be used to control the electrons accelerated up to 3 kV. G2 was always biased by dc 10 V. While G1 was first biased by dc 10 V to achieve continuous wave (cw) mode operation and then by a pulsed voltage to achieve *switching mode* operation.

In this experiment variable accelerating voltages were used in a range of 300–3000 V in steps of 300 V. At each value of accelerating voltage the emission spectrum (between 300–900 nm) was taken using a monochromator in conjunction with a cooled charge-coupled device. The observation direction for luminescence measurement was on the filament side of the VFD structure through a silicate glass window.

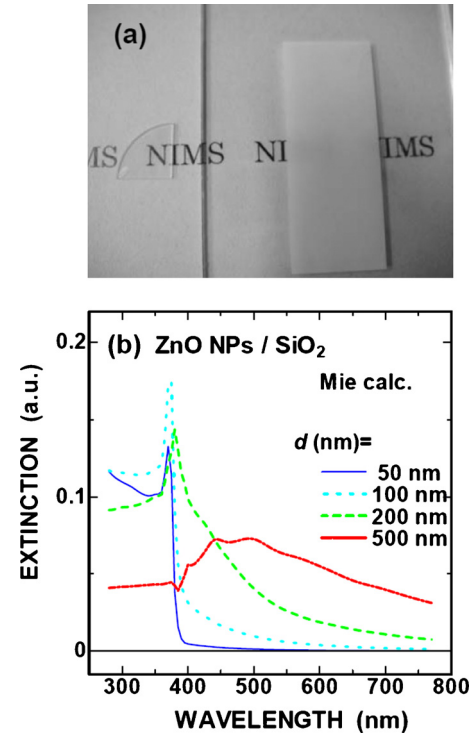


FIG. 2. (Color online) (a) Images of the ZnO NP sample (left side, transparent sector) and the conventional ZnO:Zn micropowder phosphor (right side, white rectangle) before installation into the VFD structure. (b) Optical extinction spectra of ZnO NPs of various diameters embedded in SiO<sub>2</sub> calculated by Mie's theory which assumes a dilute solution and no multiple scattering events (Ref. 8).

### III. RESULTS AND DISCUSSION

#### A. Varying appearance of new NP and conventional phosphor samples

Figure 2(a) shows images of the ZnO NP sample (left side, transparent) and the conventional ZnO:Zn micropowder phosphor (right side, white rectangle) before installation into the VFD structure. As the figure clearly shows the NP sample is transparent while the conventional phosphor is opaque. This difference is explained by Mie's theory.<sup>8</sup> Optical extinction spectra of ZnO particles of various sizes embedded in SiO<sub>2</sub> which were calculated by the Mie theory are shown in Fig. 2(b). The extinction spectrum of ZnO NPs (50 nm in diameter) shows a steep decrease around 380 nm and becomes almost zero at wavelengths longer than 400 nm. This results in the observed transparency of ZnO NPs in the visible light region. The wavelength of 380 nm corresponds to the band-edge of ZnO. However, with increasing sample diameter, the optical extinction at wavelengths longer than 380 nm, i.e. lower than the band-gap energy, increases. The extinction in this region is not due to absorption by the particles and can be attributed to scattering by the particles. When the size of particles is comparable with the wavelength of light, scattering becomes dominant. As shown in Fig. 2(b), particles of 500 nm in diameter scatter light through the whole visible region resulting in a white sample color.

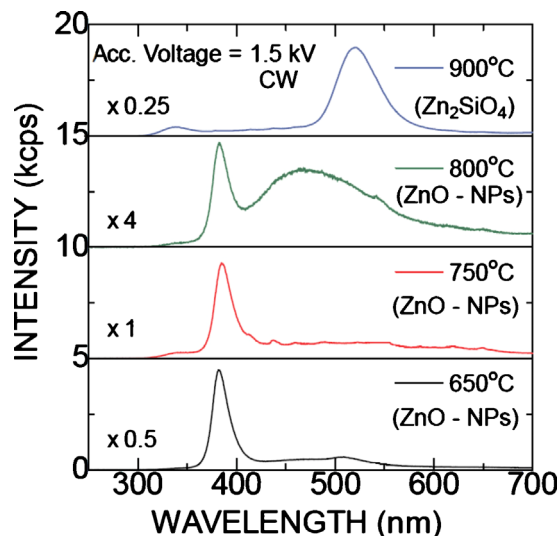


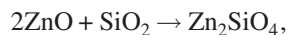
FIG. 3. (Color online) Luminescence spectra for samples annealed in an oxidizing atmosphere at varying temperatures. The spectra have been normalized and translated vertically with the addition of baselines for clarity.

### B. Spectral dependence on thermal oxidation temperature

The first important point of consideration lies in the relationship between wavelength of emitted photons and oxidation temperature. Figure 3 shows the dependence of intensity on wavelength for all four samples at a constant accelerating voltage of 1.50 kV.

Samples oxidized between 650–800 °C showed two distinct luminescence bands. First, there is a sharp peak around 380 nm which can be attributed to free-exciton recombination. Second, there is a broad band around 480 nm which can be ascribed to defect centers in ZnO NPs such as O vacancies or possibly Zn interstitials.<sup>9,10</sup> Further, with an increase in oxidation temperature, the relative intensity of the defect band increases. This behavior is consistent with the observed results of photoluminescence using the 325 nm line from a He–Cd laser as an excitation source.<sup>6,11</sup> It should be noted that the band maximum is located at ~480 nm using the VFD device structure while the maximum appears at ~500 nm under the 325 nm line excitation.<sup>6,11</sup>

The sample oxidized at 900 °C shows different behavior and emits a strong green color, corresponding to a broad peak around 520 nm. According to our previous experiments,<sup>6,7</sup> this transition can be attributed to the formation of the  $\text{Zn}_2\text{SiO}_4$  phase which is a product of the reaction between ZnO NPs and the  $\text{SiO}_2$  substrate. The formation of the  $\text{Zn}_2\text{SiO}_4$  phase has been confirmed by x-ray diffraction,<sup>7</sup> ultraviolet absorption spectroscopy,<sup>7</sup> and x-ray photoelectron spectroscopy.<sup>12</sup> According to thermodynamics data,<sup>13</sup> the reaction below is spontaneous.



$$\Delta G^\circ(T) = -31 \text{ kJ/mol}(27^\circ\text{C}) \text{ and} \\ -29 \text{ kJ/mol}(900^\circ\text{C}),$$

where  $\Delta G^\circ(T)$  denotes the standard Gibbs energy change at temperature  $T$ .

However, annealing at 900 °C or higher is required to surmount the activation energy for this reaction. Similar behavior has been observed for other ZnO nanostructures within  $\text{SiO}_2$ .<sup>14</sup> It can therefore be concluded that ZnO NPs in  $\text{SiO}_2$  are thermodynamically metastable.

It should be noted that only very weak luminescence was observed from the  $\text{Zn}_2\text{SiO}_4$  phase under He–Cd laser excitation (3.81 eV) (Ref. 11) while strong green luminescence was observed from the VFD structure. This is because  $\text{Zn}_2\text{SiO}_4$  has a wide band-gap of ~5.4 eV,<sup>7,15,16</sup> which is much larger than the energy of the 325 nm line from He–Cd laser.

While in this case an acceleration voltage of 1.50 kV was required for high intensity luminescence, this is not necessarily an intrinsic requirement. In the VFD structure high voltage is required due to the discrete nature of the ZnO NPs in conjunction with the insulating substrate. Thus only the NPs at the edge of the sample are connected to the anode via the conducting paste. This structure leads to substrate charging which electrostatically decelerates or repels further incident electrons. It is only at a relatively high voltage that this insulating barrier is surmounted. If charging could be reduced (for example, by the use of a conducting grid applied over the NPs), high intensity luminescence would be induced at a lower accelerating voltage making these devices more suitable for consumer applications.

### C. Spectral dependence on accelerating voltage

Next, the effect of varying accelerating voltage on luminescence spectra was analyzed. First the behavior using a cw gate voltage is considered followed by that of pulsed gate voltage configuration.

#### 1. Continuous wave operation

Figure 4(a) shows the series of spectra obtained from the sample oxidized at 650 °C, with varying anode (accelerating) voltage. The spectra in Fig. 4(a) show a marked shift in wavelength and a rise in intensity as accelerating voltage is increased. The increase in intensity is almost linear [Fig. 4(b)] for accelerating voltages up to 1200 V neglecting the threshold voltage of ~600 V due to substrate charging described in Sec. III B. Above 1200 V, saturation of intensity is observed. Additionally, the wavelength of the peak is significantly shifted across the upper range of voltages.

Two possible mechanisms should be considered for the redshift in the peak. The first candidate is the high-density excitation effect.<sup>17</sup> With increasing accelerating voltage the density of excitons increases and the interaction between the excitons is no longer negligible. Under high density excitation, excitons may form biexcitons or electron-hole droplets (plasma).<sup>17</sup> In fact, even at room temperature Yamamoto *et al.* observed luminescence of electron-hole plasma (EHP) from a ~200 nm thick ZnO thin film under sub-picosecond laser excitation.<sup>18</sup> Further, since our samples are NPs in origin, the confinement effect (due to restricted sample volume) of the NPs leads to an increased probability of EHP via the high-density excitation effect. According to Yamamoto *et al.*,<sup>18</sup> a free exciton peak was observed at ~376 nm under

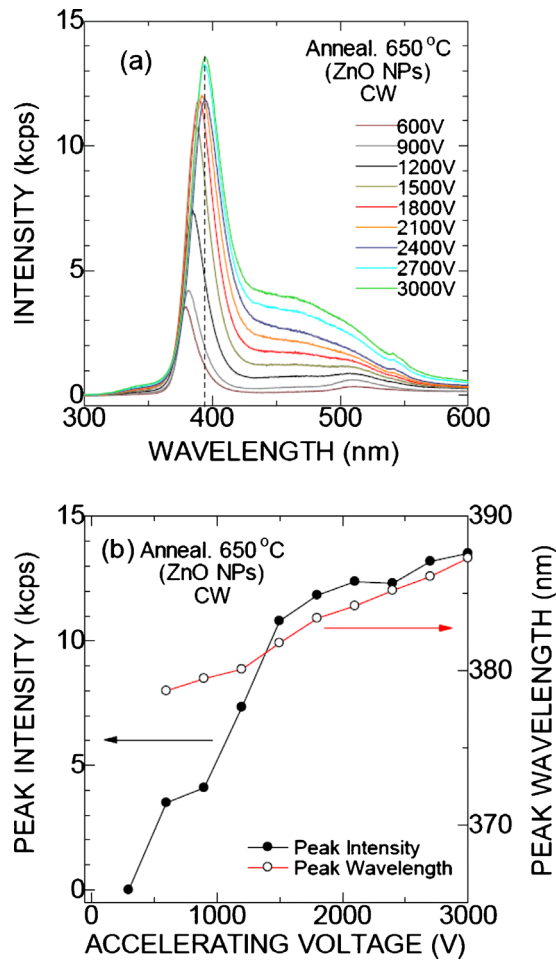


FIG. 4. (Color online) (a) Luminescence spectra obtained from sample oxidized at 650 °C. (b) Relationship between peak wavelength and intensity against accelerating voltage.

low-density excitation; but the EHP peak at ~395 nm became dominant under high-density excitation. The cross-over of these peaks with increasing accelerating voltage could account for the observed peak shift. In fact, a similar redshift and superlinear increase in PL intensity with increasing excitation was observed in ZnO:Zn micropowder under nanosecond YAG laser irradiation.<sup>2</sup>

The other candidate is the heating effect. With increased accelerating voltage, heating from the cathode ray could increase. Consequently the temperature of the sample could rise significantly. It is reported<sup>19</sup> that the free-exciton peak shows a redshift with increasing temperature following Varshni's rule:<sup>20</sup>

$$E_{\text{ex}}(T) = E_{\text{ex}}(0) - \frac{\alpha T^2}{T + \beta}, \quad (1)$$

where  $E_{\text{ex}}(T)$ ,  $E_{\text{ex}}(0)$ ,  $\alpha$ , and  $\beta$  denote the peak energy of the free-exciton emission at temperature,  $T$ , at  $T=0$  K, and two material specific fitting parameters, respectively.

Of further significance is the intensity saturation observed at accelerating voltages above approximately 1200 V. This is seemingly inconsistent with the high-density excitation effect which predicts a square dependence between excitation and intensity. However, some previous experiments

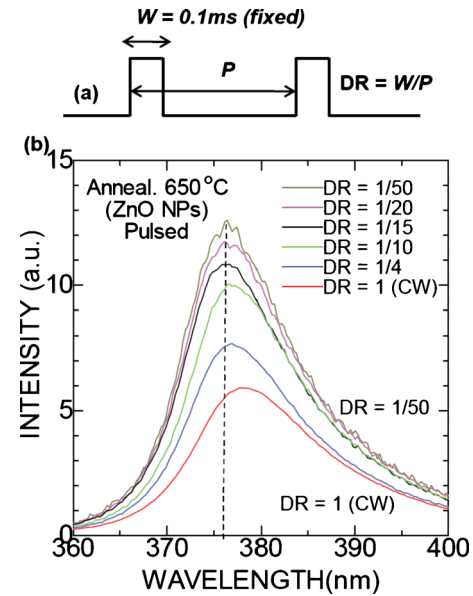


FIG. 5. (Color online) (a) Schematic diagram to show the pulse voltage applied to the sample gate, G1 in terms of voltage width (sec)  $W$  (fixed, 0.1 ms) and repetition period (sec)  $P$  (variable). (b) Luminescence spectra obtained at an accelerating voltage of 1500 V from sample oxidized at a temperature of 650 °C. Intensity values normalized by duty ratios to give cumulative intensity observed during measurement.

have reported a nearly sublinear dependence between these variables questioning the simplifications made by this theoretical basis.<sup>21</sup> The saturation is more easily explained by the heating model. With increasing temperature the luminescence efficiency decreases due to the associated thermally activated nonradiative processes.

To further examine these mechanisms, in the next part of this experiment, luminescence measurements were performed utilizing a pulsed voltage on gate G1 rather than the cw voltage. This effectively cycles the VFD on and off and thus should allow for some cooling time for the sample. Furthermore, the *on-time* was set to constant 0.1 ms which is much longer than the relaxation timescale of the high-density excitations which is typically nanoseconds or less. Consequently the high-density excitations come to a quasiequilibrium state with a pulse of 0.1 ms and therefore should have an equivalent effect on wavelength shift as in cw operation.

## 2. Pulse operation

To determine if it is sample heating that leads to a change in emitted photon wavelength pulse measurements were performed. These measurements pulse the on/off gate (G1) voltage which allows for a varying sample cooling time.

In order to determine the best source of pulse voltages, a number of duty ratios (defined as the ratio between constant voltage width (sec)  $W$  to variable repetition period (sec)  $P$  [Fig. 5(a)]) were tried to find the largest value with negligible shift in excitation wavelength. Figure 5(b) shows the spectra obtained varying duty ratio.

Considering Fig. 5 two conclusions can be drawn. First, it suggests that a decrease in duty ratio leads to convergence

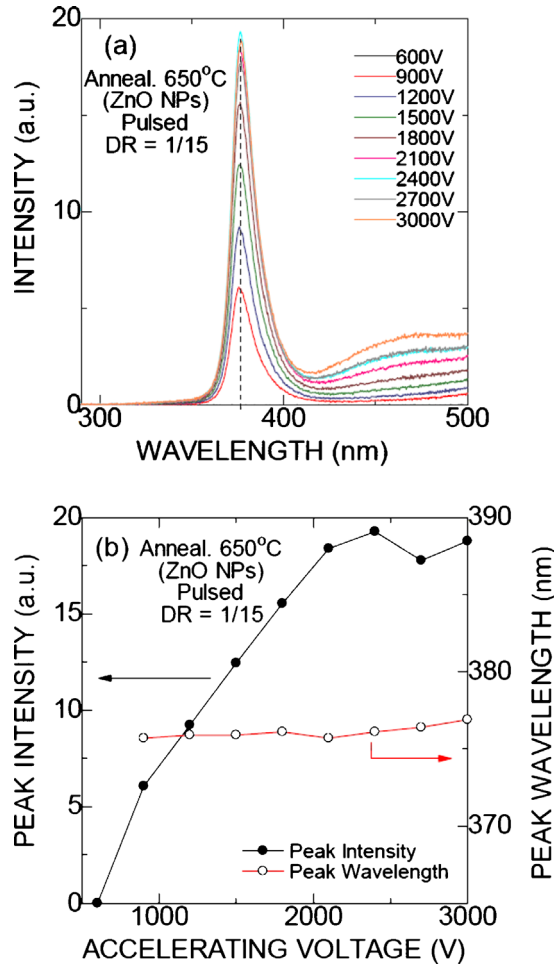


FIG. 6. (Color online) (a) Luminescence spectra obtained from sample oxidized at 650 °C using a pulsed gate voltage at DR=1/15. Intensity values normalized by duty ratio to give cumulative intensity. (b) Relationship between peak wavelength and intensity against accelerating voltage.

on a constant value of wavelength. Thus, sample heating associated with increased accelerating voltage could lead to the redshift in photons emitted.

Second, this convergence begins to occur at a duty ratio of 1/15. In Fig. 6(a) the luminescence spectra are shown for varying accelerating voltages using pulsed gate voltage at a duty ratio of 1/15. Figure 6(b) shows the peak intensity and wavelength dependences which are almost free from the heating effect.

Considering Fig. 6 it is evident that the use of a pulsed gate voltage counteracts samples heating which leads to a negligible shift in emission wavelength compared with the use of a cw gate voltage. To further explain this shift Varshni's rule [Eq. (1)] can be used to relate sample temperature to accelerating voltage. This is shown in Fig. 7.

Figure 7 helps to clarify the heating associated with an increase in accelerating voltage when a cw voltage is applied to gate G1. This heating is due to accelerated electrons continuously exciting the sample. Conversely when a pulsed voltage is applied and the sample is allowed cooling time there is very little shift in temperature across the higher values of accelerating voltage.

As shown in Fig. 6(b), the peak intensity increases almost linearly with the accelerating voltage up to 2000 V,

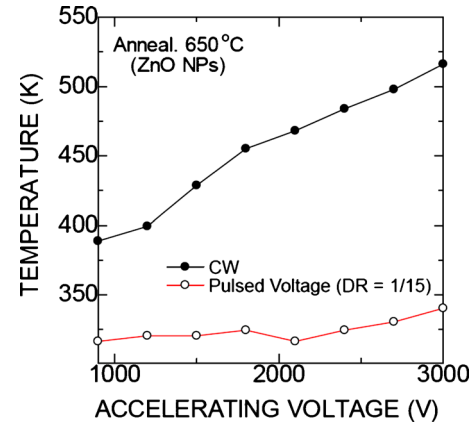


FIG. 7. (Color online) The relationship between temperature and accelerating voltage. The temperatures were derived from the exciton peak wavelengths using Varshni's rule.

neglecting the threshold voltage of  $\sim 600$  V. However, exceeding 2000 V, the intensity shows saturation. In this case the saturation cannot be attributed to thermally activated nonradiative processes because the sample temperature determined from the peak wavelength is not as high as that observed in cw mode operation. This saturation can be ascribed to the relationship between the electron penetration range and the thickness of the NP layer. Determined from cross-section TEM observations, almost all of the ZnO NPs are formed directly on the surface of the silica glass. In other words, ZnO forms a surface monolayer of NPs whose thickness is  $\sim 30$  nm.<sup>6</sup> At this energy the electron penetration range is difficult to determine. However, the range  $R$  is roughly estimated by following relationship:<sup>22</sup>

$$R[\text{cm}] = 7.4 \times 10^{-6} \frac{(E[\text{keV}])^{1.49}}{\rho[\text{g/cm}^3]} \quad (0.37 \text{ keV} < E < 10 \text{ keV}), \quad (2)$$

where  $E$  and  $\rho$  denote the acceleration energy in the units of kiloelectron volts and the mass-density of the target material in units of grams per cubic centimeter respectively. The mass-density of ZnO NPs was taken as a bulk value of  $5.70 \text{ g/cm}^3$ . The electron ranges calculated by Eq. (2) are summarized in Table I. Exceeding 2 keV, the electron penetration range becomes larger than the thickness of ZnO NP layer  $\sim 30$  nm. This leads to lower excitation efficiency in the ZnO NP layer and the observed intensity saturation.

TABLE I. Electron penetration ranges in ZnO implanted structure at given accelerating voltages calculated from Eq. (2).

Accelerating voltage (kV)	Electron range (nm)
0.5	5
1.0	13
1.5	24
2.0	36
2.5	51
3.0	67
Thickness of ZnO NP layer: $\sim 30$ nm.	

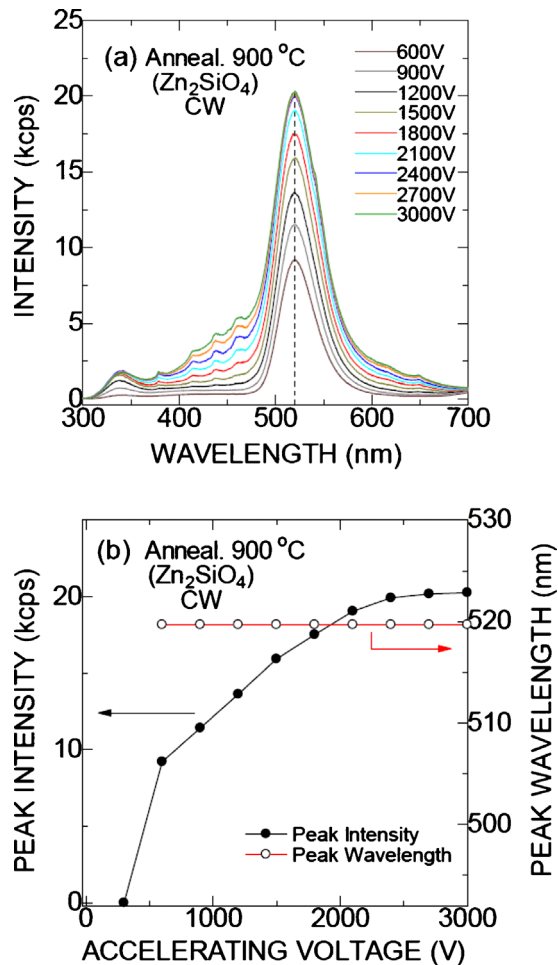


FIG. 8. (Color online) (a) Luminescence spectrum obtained from sample oxidized at 900 °C at varying values of accelerating voltage. (b) Relationship between peak wavelength and intensity against accelerating voltage.

#### D. High temperature oxidation product ( $\text{Zn}_2\text{SiO}_4$ phase)

As shown in Fig. 3, high temperature oxidation at 900 °C leads to a strong shift in the luminescence peak wavelength. Amekura *et al.*<sup>7</sup> have shown that this is due to the formation of the zinc silicate phase,  $\text{Zn}_2\text{SiO}_4$ . In order to understand how a change in accelerating voltage affected photon emission from this structure, luminescence spectra were taken using the same experimental methodology as in part (B) under cw operation. They are displayed in Fig. 8.

In Fig. 8 it is observed that similar to the first sample an increase in accelerating voltage leads to an increase in intensity up to saturation. However, there is no shift in peak wavelength. This is in strong contrast with the exciton luminescence shown in Fig. 4.

Previous experiments suggest that the  $\text{Zn}_2\text{SiO}_4$  phase has a wide band-gap of  $\sim 5.4$  eV.<sup>7</sup> However the luminescence peak appears at 520 nm (2.4 eV). This is because it is certain deeper level energy transitions rather than near-band gap transitions that are responsible for photon emission. It seems that these deep level centers are unaffected by changes in temperature and therefore the emission peak is free from thermally induced shift. The temperature-independent

emission-wavelength in cw operation observed from this structure could be attractive for certain applications.

#### IV. CONCLUSIONS

ZnO NPs were used to substitute conventional phosphor powder inside VFDs. The luminescent spectra observed were strongly dependent on sample annealing temperature. Samples that comprised of ZnO NPs showed a shift in exciton peak wavelength as accelerating voltage was increased. This was due to sample heating which led to a decrease in luminescence efficiency through associated thermally activated nonradiative processes. Even at increased temperatures (up to 520 K) strong luminescence was observed which is attractive in certain applications. Sample heating and the associated shift in exciton peak wavelength were mitigated through the use of a pulsed gate voltage which allowed for increased sample cooling time. Even using the pulsed mode operation, saturation intensity was still observed exceeding accelerating voltages of 2 kV. This behavior can be attributed to the nanometric thickness ( $\sim 30$  nm) of the ZnO NP layer, which becomes shorter than the electron range at high voltages exceeding 2 kV. The thermally induced peak shift was absent from the sample based on the high temperature oxidation product,  $\text{Zn}_2\text{SiO}_4$ , as the associated luminescence centers are of a deeper level.

#### ACKNOWLEDGMENTS

The authors would like to thank Mr. Y. Yonezawa (Futaba Corporation) for his encouragement of collaborative research. C.H.A and H.A would also like to thank IAESTE (The International Association for the Exchange of Students for Technical Experience) for organizing the internship which allowed this experimental session to take place.

- <sup>1</sup>J. A. Castellano, *Handbook of Display Technology* (Academic, San Diego, 1992).
- <sup>2</sup>M. Ichimiya, T. Horii, T. Hirai, Y. Sawada, M. Minamiguchi, N. Ohno, M. Ashida, and T. Ito, *J. Phys.: Condens. Matter* **18**, 1967 (2006).
- <sup>3</sup>K. Vanheusden, W. L. Warren, C. H. Seager, D. R. Tallant, J. A. Voigt, and B. E. Gnade, *J. Appl. Phys.* **79**, 7983 (1996).
- <sup>4</sup>H. Amekura and N. Kishimoto, in *Lecture Notes in Nanoscale Science and Technology* edited by Z. Wang (Springer, New York, 2009), Vol. 5, pp. 1–75.
- <sup>5</sup>J. Chen, R. Mu, A. Ueda, M. H. Wu, Y.-S. Tung, Z. Gu, D. O. Henderson, C. W. White, J. D. Budai, and R. A. Zuhur, *J. Vac. Sci. Technol. A* **16**, 1409 (1998).
- <sup>6</sup>H. Amekura, N. Umeda, Y. Sakuma, O. A. Plaksin, Y. Takeda, N. Kishimoto, and C. Buchal, *Appl. Phys. Lett.* **88**, 153119 (2006).
- <sup>7</sup>H. Amekura, K. Kono, N. Kishimoto, and C. Buchal, *Nucl. Instrum. Methods Phys. Res. B* **242**, 96 (2006).
- <sup>8</sup>G. Mie, *Ann. Phys.* **330**, 377 (1908) (in German).
- <sup>9</sup>U. Özgür, Y. I. Alivov, C. Liu, A. Teke, M. A. Reschikov, S. Dogan, V. Avrutin, S.-J. Cho, and H. Morkoc, *J. Appl. Phys.* **98**, 041301 (2005).
- <sup>10</sup>H. Zeng, G. Duan, Y. Li, S. Yang, X. Xu, and W. Cai, *Adv. Funct. Mater.* **20**, 561 (2010).
- <sup>11</sup>H. Amekura, Y. Sakuma, K. Kono, Y. Takeda, N. Kishimoto, and C. Buchal, *Physica B* **376–377**, 760 (2006).
- <sup>12</sup>H. Amekura, O. A. Plaksin, M. Yoshitake, Y. Takeda, N. Kishimoto, and C. Buchal, *Appl. Phys. Lett.* **89**, 023115 (2006).
- <sup>13</sup>O. Kubaschewski, E. L. Evans, and C. B. Alcock, *Metallurgical Thermodynamics*, 4th ed. (Pergamon, London, 1967).
- <sup>14</sup>J. G. Ma, Y. C. Liu, C. S. Xu, Y. X. Liu, C. L. Shao, H. Y. Xu, J. Y. Zhang, Y. M. Lu, D. Z. Shen, and X. W. Fan, *J. Appl. Phys.* **97**, 103509 (2005).
- <sup>15</sup>S. Z. Karazhanov, P. Ravindran, H. Fjellvag, and B. G. Svensson, *J. Appl.*

- [Phys.](#) **106**, 123701 (2009).
- <sup>16</sup>H. Chang, H. D. Park, K. S. Sohn, and J. D. Lee, *J. Korean Phys. Soc.* **34**, 545 (1999).
- <sup>17</sup>N. Peyghambarian, S. W. Koch, and A. Mysyrowicz, *Introduction to Semiconductor Optics* (Prentice Hall, New Jersey, 1993).
- <sup>18</sup>A. Yamamoto, T. Kido, T. Goto, Y. Chen, T. Yao, and A. Kasuya, *J. Cryst. Growth* **214–215**, 308 (2000).
- <sup>19</sup>L. Wang and N. C. Giles, *J. Appl. Phys.* **94**, 973 (2003).
- <sup>20</sup>Y. P. Varshni, *Physica* **34**, 149 (1967).
- <sup>21</sup>T. Baba and T. Masumi, *J. Phys. Soc. Jpn.* **56**, 2549 (1987).
- <sup>22</sup>Y. Yamazaki, *Particle Beam Physics* (Maruzen, Tokyo, 1994) (in Japanese).